

^{129}Xe -Rb Spin-Exchange Optical Pumping with High Photon Efficiency

G. Norquay, G. J. Collier, M. Rao, N. J. Stewart, and J. M. Wild

POLARIS, Academic Unit of Radiology, Department of Infection, Immunity and Cardiovascular Disease, University of Sheffield, Sheffield, South Yorkshire, United Kingdom (Received 5 April 2018; published 8 October 2018; corrected 28 January 2019 and 31 December 2020)

Here we present a Rb- ^{129}Xe spin-exchange optical pumping polarizer capable of rapid generation of large volumes of highly polarized ^{129}Xe gas. Through modeling and measurements we maximize the ^{129}Xe nuclear spin polarization output to enable the generation of polarized ^{129}Xe gas imaging volumes (300 cm³) every 5 min within a clinical setting. Our model is verified by experiment to correctly predict the optimum Rb vapor density for maximum ^{129}Xe nuclear polarization for a flux 3.4 W/cm² of circularly polarized Rb D_1 photons incident on an 80 cm long cylindrical optical cell. We measure a ^{129}Xe magnetization production efficiency of $\eta_{\text{pr}} = 1.8\%$, which approaches the photon efficiency limit $\eta_{\gamma} = 3.3\%$ of this system and enables the polarization of 2.72×10^{22} ^{129}Xe spins per hour, corresponding to 1013 cm³ of 100% polarized ^{129}Xe at STP. This magnetization production rate is threefold higher than the highest previously published ^{129}Xe magnetization production rate and has enabled routine clinical lung magnetic resonance imaging (MRI) with hyperpolarized ^{129}Xe doses available on demand at run time, as well as high-SNR ^{129}Xe MRI of the human brain and kidneys.

DOI: [10.1103/PhysRevLett.121.153201](https://doi.org/10.1103/PhysRevLett.121.153201)

The ability to generate highly magnetized ^{129}Xe gas with spin-exchange optical pumping (SEOP) [1] benefits scientific study in many fields, including fundamental symmetry tests [2,3], chemical physics [4], materials science [5], and biomedical magnetic resonance imaging (MRI) [6]. Despite technological advances [7–9], a limiting factor in the widespread application of hyperpolarized ^{129}Xe has been the difficulty in rapidly generating large volumes of ^{129}Xe with high nuclear polarization P_{Xe} for clinical MRI and other applications where high ^{129}Xe throughput is required.

In Rb- ^{129}Xe SEOP, spin angular momentum of left circularly polarized photons is transferred to D_1 line valence electrons within vaporized Rb, generating a polarized Rb spin population. The electronic Rb spin polarization is then transferred to ^{129}Xe nuclei through the collisional Fermi-contact hyperfine interaction, resulting in a “hyperpolarized” ^{129}Xe nuclear spin system. A useful concept in the evaluation of SEOP physics is the photon efficiency η_{γ} , which is defined as the number of polarized nuclei per photon absorbed by Rb vapor. In practical terms, it is related to the ^{129}Xe magnetization output (polarization-volume product) of a SEOP system and may be described as the ratio of ^{129}Xe spin polarization rate to the photon absorption rate $\Delta\Phi$ within a SEOP cell volume V [10,11]

$$\eta_{\gamma} = \frac{V[\text{Xe}]dP_{\text{Xe}}/dt}{\Delta\Phi} = \frac{P_{\text{Xe}}^{\text{eq}}[\text{Xe}]V}{\Delta\Phi\tau_{\text{up}}}, \quad (1)$$

where $[\text{Xe}]$ denotes the Xe number density within the cell volume, $P_{\text{Xe}}^{\text{eq}}$ is the equilibrium ^{129}Xe polarization, and τ_{up}

is the time constant characterizing the time for ^{129}Xe nuclei to reach a polarization equilibrium. Measurements performed at low laser power [8–10] determined η_{γ} for ^{129}Xe -Rb to be approximately 0.04, meaning an average of 25 photons are required to polarize a single ^{129}Xe nucleus. Practically, this translates to a magnetization output rate of 21 cm³ h⁻¹ of 100% polarized ^{129}Xe per watt of absorbed light. (N.B.: Throughout this Letter, magnetization output rates will be normalized assuming 100% ^{129}Xe polarization, 100% ^{129}Xe isotopic enrichment, and operation at STP.) With diodes capable of producing 100s of watts of light at the Rb D_1 wavelength now readily available, it should therefore be possible to achieve magnetization output rates of the order 1000 cm³ h⁻¹. However, owing to prior employment of relatively small SEOP cell volumes (75 cm³ [12] to 1500 cm³ [13]), these outputs have not yet been realized on practical SEOP systems, with published ^{129}Xe magnetization output rates to date in the range 39 to 240 cm³ h⁻¹ [14].

This Letter describes a continuous-flow ^{129}Xe SEOP system which was designed with a large SEOP cell volume $V = 3530$ cm³ in order to maintain high photon efficiency and overcome previous magnetization output limitations. We also present a practical SEOP physics model with the aim of determining the experimental parameters that satisfy the design criterion that maximizes photon efficiency, namely, achieving 100% photon absorption without any optically dark regions over the cell length. We then compare our model against experimental measurements and use the optimized parameters to enable rapid generation of polarized

^{129}Xe for high-quality MR imaging of hyperpolarized ^{129}Xe in human lungs, brain, and kidneys.

During Rb- ^{129}Xe SEOP, the spin angular momentum of left circularly polarized photons ($s_z = +\hbar$) is absorbed by the Rb vapor at a rate $\delta\Gamma = (1 - P_{\text{Rb}})R_p$ per Rb atom, where P_{Rb} is the Rb electron polarization, and R_p is the optical pumping rate (photon absorption rate for unpolarized Rb atoms). The attenuation of the photon flux $\Phi = P_I n_p / A$ (where P_I is the laser power over beam area A , and n_p is the number of photons per joule at the pump beam wavelength λ_l) over the length z of the SEOP cell may be written as a nonlinear differential equation for R_p as $dR_p(z)/dz = -\beta[1 - P_{\text{Rb}}(z)]R_p(z)$ [15]. $P_{\text{Rb}}(z) = R_p(z)/(R_p(z) + \Gamma_{\text{SD}})$ is the time-averaged Rb electron polarization at cell position z , Γ_{SD} is the Rb spin-destruction rate and $\beta = \alpha[\text{Rb}]$ is a function of Rb vapor density [Rb] (dependent upon SEOP cell temperature) with the constant α (units cm^2), which relates the optical pumping rate and photon flux [16] via

$$R_p = \frac{2\sqrt{\pi} \ln 2 r_e f_{D_1} \lambda_l^3 w'(r, s) P_I n_p}{hc \Delta\lambda_l n_p} \frac{P_I n_p}{A} = \alpha \Phi. \quad (2)$$

Here r_e is the classical electron radius, f_{D_1} is the oscillator strength of the Rb D_1 transition, c is the speed of light, $\Delta\lambda_l$ is the pump beam linewidth, and $w'(r, s)$ is the real part of the complex overlap function (defined by $w = w' + iw'' = e^{\ln 2(r+is)^2} \text{erfc}[\sqrt{\ln 2}(r+is)]$) [17], for which $r = \Delta\nu_a / \Delta\nu_l$ ($\Delta\nu_l = c\Delta\lambda_l / \lambda_l^2$) represents the relative atomic linewidth and $s = 2(\nu_l - \nu_a) / \Delta\nu_l$ is the relative detuning ($s = 0$ for $\nu_l = \nu_a$), where ν_a and $\Delta\nu_a$ are the center frequency and linewidth of the Rb D_1 absorption line, respectively. To enable optimization of R_p and P_{Rb} for different cell geometries and SEOP conditions, we obtain an explicit solution of R_p over z ,

$$R_p(z) = \Gamma_{\text{SD}} W(e^{(k-\beta z)} / \Gamma_{\text{SD}}), \quad (3)$$

where W is the Lambert-W function defined such that for an arbitrary function $f(x) = xe^x$, $W(f(x)) = x$, and $k = \ln(R_{p0}) + R_{p0} / \Gamma_{\text{SD}}$ is the boundary constant determined at $z = 0$, where R_{p0} is calculated using Eq. (2).

Figure 1(c) shows modeled longitudinal R_p and P_{Rb} profiles along the SEOP cell at an optimized temperature $T = 398$ K and suboptimal profiles at a cell temperature just 10 K higher for a cylindrical cell of volume $V = 3530$ cm^3 (7.5 cm diameter, 80 cm length) with parameters optimized using Eq. (3): $P_I = 150$ W pump beam with $\lambda_l = 794.77$ nm and $\Delta\lambda_l = 0.3$ nm incident on the cell filled to a gas density $[G] = 0.847$ amg (3% Xe, 10% N_2 , 87% He). Rb densities [Rb] were calculated indirectly using Rb vapor pressure curves reported by Killian [18]. Rb spin destruction Γ_{SD} occurs either in binary collisions between Rb and Xe atoms or in bound RbXe van der Waals (VDW) molecules,

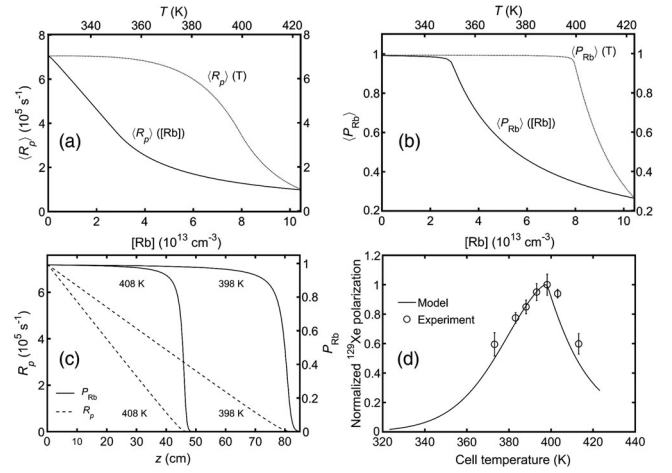


FIG. 1. (a) and (b) show the average optical pumping rate $\langle R_p \rangle$ and Rb polarization $\langle P_{\text{Rb}} \rangle$ over the cell as functions of cell temperature and Rb vapor density, and (c) shows the modeled optical pumping rate R_p and Rb polarization P_{Rb} as a function of SEOP cell length for two cell temperatures $T = 398$ and 408 K using Eq. (3). (d) Comparison of modeled [Eq. (6)] and experimentally measured ^{129}Xe polarizations as a function of SEOP cell temperature. The measurements were made using gas extracted from a cylindrical SEOP cell with volume $V = 3530$ cm^3 (7.5 cm diameter, 80 cm length) during continuous-flow SEOP at a total gas flow rate of 2000 sccm and a cell pressure of 938 Torr.

and the total Rb spin-destruction rate is given by a sum of the two contributions $\Gamma_{\text{SD}} = \Gamma_{\text{SD}}^b + \Gamma_{\text{SD}}^v$. The binary Rb spin-destruction rate is defined as $\Gamma_{\text{SD}}^b = \langle \sigma v \rangle_{\text{SD}} [\text{Xe}]$, where $\langle \sigma v \rangle_{\text{SD}} = 7.44 \times 10^{-15} (T/373)^{1.17}$ cm^3/s is the measured temperature-dependent binary Rb spin-destruction cross section [19]. It is not possible to accurately describe spin destruction occurring in RbXe VDW molecules with a simple cross section owing to the three-body nature of the formation and breakup of the RbXe VDW molecules [20]. Previous measurements of the VDW spin-destruction rates are specific to the gas composition used in each study, making it difficult to predict spin-destruction rates due to VDW molecules for a specific gas composition. We have therefore derived expressions that enable calculation of VDW Rb spin-destruction rates for any gas (Xe, N_2 , He)/Rb isotopic composition. The VDW spin-destruction rate may be defined by $\Gamma_{\text{SD}}^v = |q(F, F)| / T_F$ [20,21], where $T_F^{-1} = [\text{Xe}] k \tau^{-1}$ is the RbXe molecular formation rate per Rb atom, $|q(F, F)|$ is the probability that the Rb spin polarization will be lost during the characteristic lifetime τ of a VDW molecule, and $k = [\text{RbXe}] / [\text{Xe}][\text{Rb}] = 244 \text{ \AA}^3 (T/373)^{-3/2}$ is the molecular chemical equilibrium constant [22]. The molecular lifetime τ of RbXe molecules is inversely proportional to the gas density of the third body $[G]_i$ ($i = \text{Xe}, \text{N}_2, \text{He}$), and we have derived an expression to enable calculation of τ for an arbitrary gas composition

$$\frac{1}{\tau} = \frac{\omega_\gamma}{\phi_\gamma} = \sum_i \frac{\gamma N}{\hbar} \frac{[G]_i}{[G]_{0,i}}, \quad (4)$$

where $\omega_\gamma = \gamma N / \hbar = 754 \text{ rad}^6/\text{s}$ [23] is the spin-rotation frequency of the Rb electron spin vector \mathbf{S} about the rotational angular momentum vector \mathbf{N} of the RbXe molecule, ϕ_γ is the phase angle subtended by \mathbf{S} within a molecular lifetime τ , and γ is the coupling constant that determines the strength of the spin-rotation interaction $\gamma \mathbf{N} \cdot \mathbf{S}$ [21]. $[G]_{0,i}$ defined as the characteristic third-body density for which the phase angle ϕ_γ is unity has been previously measured for He and N_2 to be $[G]_{0,\text{He}} = 0.172 \text{ amg}(373/T)^{1/2}$ and $[G]_{0,\text{N}_2} = 0.105 \text{ amg}(373/T)^{1/2}$ [24] and has been calculated for Xe to be $[G]_{0,\text{Xe}} = 0.028 \text{ amg}(373/T)^{1/2}$ [25,26]. Here we generalize the VDW spin-destruction probability $|q(F, F)|$ from Eq. (26) in Ref. [20] to be valid for any Rb isotopic composition

$$|q(F, F)| = \frac{2}{3} \left[\sum_i \eta_i \left(\frac{\phi_\gamma}{(2I_i + 1)} \right)^2 \right] \left(1 + \frac{K(K+1)}{x^2} f \right), \quad (5)$$

where the sum contains two terms corresponding to the two naturally occurring isotopes of Rb, ^{85}Rb and ^{87}Rb , that occur with isotopic fractions $\eta_1 = 0.7215$ and $\eta_2 = 0.2785$ and that have nuclear spin numbers $I_1 = 5/2$ and $I_2 = 3/2$, respectively. $x = \gamma N / \alpha = 4.1$ [10] is the Breit-Rabi field parameter and determines the fractions of Rb electronic spin S momentum that is transferred to rotational angular momentum N and to ^{129}Xe nuclear spin $K = 1/2$. α is the coupling strength for the collisional Fermi-contact hyperfine interaction $\alpha \mathbf{K} \cdot \mathbf{S}$ between the ^{129}Xe nuclear spin \mathbf{K} and the Rb electron spin \mathbf{S} , and f is the isotopic fraction of ^{129}Xe . Equation (5) is valid in the limit of sufficiently high third-body gas densities that holds for all of this work (0.33–1.33 amg) where $\phi_\gamma / (2I + 1) \ll 1$.

The polarizer system comprises five main components: (i) a laser-diode array coupled with polarizing and beam shaping optics, (ii) an oven containing a long cylindrical optical cell, (iii) an electromagnetic coil assembly, (iv) a gas-handling manifold, and (v) a cryostat within a permanent magnetic field. See Fig. 3(a) for a schematic of the apparatus and the Supplemental Material [27] for a full description of all components. The light for optical pumping was generated by a laser-diode array (QPC Lasers) set to output circularly polarized laser light $P_l = 150 \text{ W}$ tuned to $\lambda_l = 794.77 \text{ nm}$ with a narrow linewidth $\Delta\lambda_l = 0.3 \text{ nm}$ and a circular spatial beam profile with a diameter of 7.5 cm ($3.4 \text{ W}/\text{cm}^2$). The oven is composed of calcium silicate blocks and contains borosilicate windows with antireflection coating (at 795 nm) and a cylindrical borosilicate cell with volume $V = 3530 \text{ cm}^3$ (80 cm length, 7.5 cm diameter) loaded with $< 1 \text{ g}$ of natural abundance Rb. To regulate the Rb vapor density, the oven is heated with

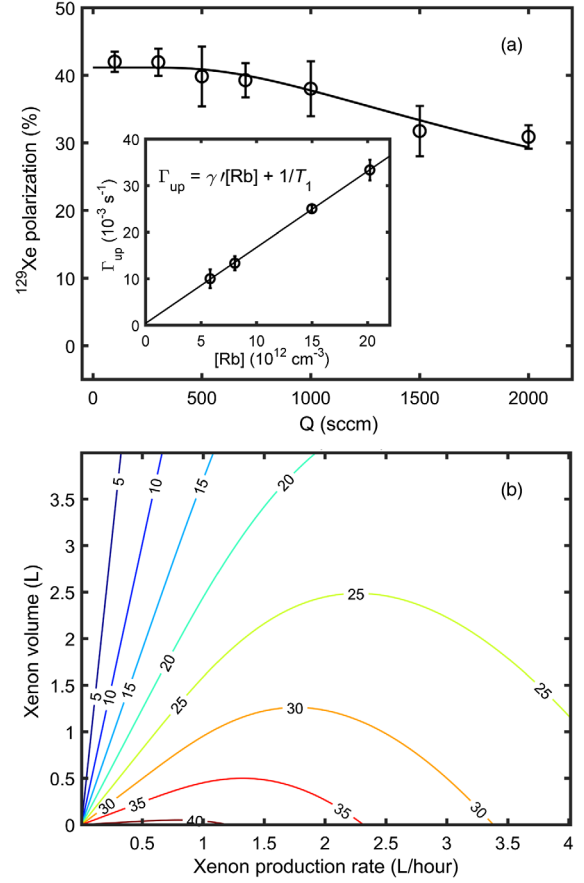


FIG. 2. (a) Measured ^{129}Xe polarization as a function of total gas flow rate Q through the SEOP cell. Equation (6) was fit to the data to determine a spin-up time $\tau_{\text{up}} = 1/(\gamma_{\text{SE}} + \Gamma) = 71 \text{ s}$. Inset is a series of measurements of the spin-up rate $\Gamma_{\text{up}} = 1/\tau_{\text{up}}$ made on the cell under static conditions (zero gas flow) at different Rb vapor densities $[\text{Rb}]$ to determine a spin-exchange cross section $\gamma' = 1.63 \times 10^{-15} \text{ cm}^3/\text{s}$ and the ^{129}Xe spin-relaxation rate $\Gamma = 1/T_1 = (44 \times \text{min})^{-1}$ in the absence of Rb vapor. (b) ^{129}Xe polarization production map: contour plot of P_{Xe} (in %) for a given volume of Xe at different production rates.

air that is passed through a heating element temperature controlled using a thermocouple situated within the oven air space. The oven is contained within a homogeneous magnetic field $B_0 = 30 \text{ G}$ ($\Delta B_0 < 1\%$ over cell length) generated by a four-coil electromagnet using square coils with side lengths of 100 cm and geometrical configuration based on Ref. [28]. During continuous-flow operation, the gas manifold directs gas flow from a cylinder containing 3% isotopically enriched Xe (86% ^{129}Xe), 10% N_2 , and 87% He through the cell in a direction counter to the laser propagation. The gas exiting the cell is flowed through Tygon tubing towards spiral glassware held within a field of 2.5 kG (NdBFe permanent magnet) and submerged in a dewar containing liquid N_2 , whereupon the Xe is cryogenically separated from He and N_2 , which are removed as exhaust gases through a vacuum line. All ^{129}Xe polarization measurements were performed *in situ* within the bore of a

1.5 T GE MRI scanner as described previously [8]. Each polarization measurement corresponds to the mean signal value from NMR measurements taken from five separate cell dispenses for given running parameters (e.g., cell pressure, cell temperature, and gas flow rate). The relationship [29]

$$P_{Xe} = \langle P_{Rb} \rangle \frac{\gamma_{SE}}{\gamma_{SE} + \Gamma} (1 - e^{-(\gamma_{SE} + \Gamma)t_r}) \quad (6)$$

was used to model the ^{129}Xe polarization during gas flow Q through the SEOP cell. $\langle P_{Rb} \rangle$ is the average Rb polarization over the SEOP cell volume (see Fig. 1(b) for $\langle P_{Rb} \rangle$ as a function of cell temperature T and $[\text{Rb}]$), $\gamma_{SE} = \gamma_{SE}^v + \gamma_{SE}^b$ is the total spin-exchange rate, Γ is the ^{129}Xe relaxation rate in the absence of Rb vapor (see Fig. 2(a) inset), and $t_r = [G]V/Q$ is the atomic residency time in the SEOP cell volume V . The Rb- ^{129}Xe binary spin-exchange rate is independent of gas density and is defined as $\gamma_{SE}^b = \langle \sigma v \rangle_{SE} [\text{Rb}]$, where $\langle \sigma v \rangle_{SE} = 2.17 \times 10^{-16} \text{ cm}^3/\text{s}$ is the experimentally determined binary spin-exchange cross section [30]. The VDW spin-exchange rate γ_{SE}^v may be defined analogously to the Rb VDW spin-destruction rate as $\gamma_{SE}^v = |q(K, K)|/T_K$, where $T_K^{-1} = [\text{Rb}]k\tau^{-1}$ is the RbXe molecular formation rate per Xe atom, and $|q(K, K)|$ is the probability of spin exchange occurring during the lifetime τ of a VDW molecule [Eq. (4)]

$$|q(K, K)| = \frac{2}{3} \left[\sum_i \eta_i \left(\frac{\phi_\gamma}{(2I_i + 1)x} \right)^2 \right] \times \left[\sum_i \eta_i [I_i(I_i + 1)] + \frac{3}{2} \right]. \quad (7)$$

The highest P_{Xe} during gas flow $Q = 2000 \text{ sccm}$ and a cell pressure of 938 Torr was measured at a cell temperature $T = 398 \text{ K}$ ($[G] = 0.847 \text{ amg}$), in excellent agreement with our model, as shown in Fig. 1(d). We observed a minimal dependence of P_{Xe} on total cell pressure within the range 375–2250 Torr, in agreement with previous measurements performed under flow conditions [13]. The coefficient of the exponential in Eq. (6) $\langle P_{Rb} \rangle \gamma_{SE}/(\gamma_{SE} + \Gamma)$ represents the ^{129}Xe polarization P_{Xe}^{eq} for an infinite residency time $t_r = \infty$ (i.e., gas flow $Q = 0$), and the spin-up time constant in Eq. (1) may be represented by the reciprocal of the exponential rate constant, i.e., $\tau_{\text{up}} = 1/(\gamma_{SE} + \Gamma)$ for $t_r < \infty$. Figure 2(a) shows a fit of Eq. (6) to gas flow data yielding $\tau_{\text{up}} = 71 \text{ s}$ and $P_{Xe}^{\text{eq}} = 41\%$. The predicted value of P_{Xe} from Eq. (6) is a factor of 2 higher than our experimental values, which is consistent with previous observations during continuous-flow Rb- ^{129}Xe SEOP [13,31]. This may be due to an incomplete understanding of SEOP physics as has been previously observed in the case of Rb- ^3He [32]; however it is beyond the scope of this Letter to attempt to resolve the widely reported discrepancy between theoretical and experimental ^{129}Xe polarization values. To generate hyperpolarized ^{129}Xe production maps, the experimental data in Fig. 2(a) were combined with a model of ^{129}Xe polarization decay during the cryogenic accumulation process [8,29]. The production

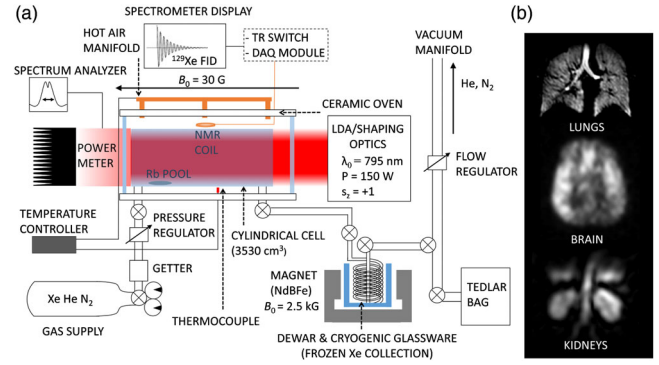


FIG. 3. (a) Schematic of the key functional components of the Rb- ^{129}Xe polarizer and (b) magnetic resonance images of hyperpolarized ^{129}Xe gas in human lungs and dissolved-phase ^{129}Xe in the human brain [33] and kidneys [34].

map shown in Fig. 2(b) illustrates that the system is capable of generating 300 cm^3 of Xe with $P_{Xe} \approx 30\%$ in 5 min ($Q_{Xe} = 3.6 \text{ L h}^{-1}$), which enables on-demand production of gas for several imaging sequences per patient lung MRI exam in a clinical setting. Figure 3(b) shows examples of high-quality human lung, brain, and kidney MR imaging with hyperpolarized ^{129}Xe produced at $Q_{Xe} = 3.6 \text{ L h}^{-1}$. To enable an estimation of the photon efficiency η_γ [Eq. (1)], we measured the photon absorption rate $\Delta\phi$ in the cell volume at a gas flow rate $Q = 2527 \text{ sccm}$ such that the atomic residency time t_r is equal to the experimentally measured spin-up time $\tau_{\text{up}} = 71 \text{ s}$. The photon absorption rate was calculated using $\Delta\phi = (P_c - P_h)/E_p = 4.20 \times 10^{20} \text{ s}^{-1}$, where $P_c = 120 \text{ W}$ and $P_h = 15 \text{ W}$ are the measured laser powers after transmission through the cell at room temperature (zero $[\text{Rb}]$) and at a temperature $T = 398 \text{ K}$, respectively, and $E_p = 2.50 \times 10^{-19} \text{ J}$ is the energy of a photon at the Rb D_1 resonance $\lambda_a = 794.77 \text{ nm}$. With a Xe density $[\text{Xe}] = 6.83 \times 10^{17} \text{ cm}^{-3}$ and $P_{Xe}^{\text{eq}} = 0.41$ [$Q = 0 \text{ sccm}$ in Fig. 2(b)], Eq. (1) is used to calculate a photon efficiency of $\eta_\gamma = 0.033$, which means that on average 30 photons are required to polarize a single ^{129}Xe nucleus on this system, which translates to a magnetization output rate of $17.7 \text{ cm}^3 \text{ h}^{-1}$ per watt of absorbed light.

It is worth noting that this magnetization output rate is not practically achievable on a system during operation as in Eq. (1) the ^{129}Xe polarization P_{Xe}^{eq} is defined at $t = \infty$, whereas during operation the ^{129}Xe polarization is defined for a gas residency time $t_r = [G]V/Q$. For an operating flow rate of $Q = 2000 \text{ sccm}$ (where $Q_{Xe} = 3.6 \text{ L h}^{-1}$), $t_r = 90 \text{ s}$ and the postthaw (5 min accumulation) ^{129}Xe polarization is $P_{Xe} = 0.29$. Substituting $t_r = 90$ and $P_{Xe} = 0.29$ for τ_{up} and P_{Xe}^{eq} in Eq. (1), respectively, enables us to calculate a “production efficiency” $\eta_{\text{pr}} = 0.018$, which corresponds to a magnetization output rate of $1013 \text{ cm}^3 \text{ h}^{-1}$ for 105 W of absorbed light. This value is 4.6-fold and 2.9-fold higher than the highest previously published magnetization output rates of $220 \text{ cm}^3 \text{ h}^{-1}$ [35] and $352 \text{ cm}^3 \text{ h}^{-1}$

[7] on stopped- and continuous-flow Rb- ^{129}Xe polarizers, respectively, and has enabled routine clinical lung MRI with hyperpolarized ^{129}Xe doses available on demand at run time, as well as high-SNR ^{129}Xe MRI of the human brain and kidneys. In addition, the high magnetization output rate has opened up the possibility to perform lung MRI with naturally abundant Xe (26% ^{129}Xe) at higher doses, which, owing to the much lower cost when compared to enriched Xe [36], should further enhance the potential for large-scale clinical dissemination of hyperpolarized ^{129}Xe MRI.

Further work incorporating direct measurements of the Rb density along the cell and P_{Xe} , P_{Rb} measurements along the transverse plane of the cell is under way to provide insight into the discrepancy between theoretical and experimental P_{Xe} , which should enable further optimization of the polarizer's performance.

The authors are grateful to Daniel Jackson for blowing the SEOP cells and to Simon Wiles and John Wilson for assistance with construction of the polarizer. This work was supported by UK EPSRC Grant No. EP/D070252/1, NIHR Grant No. NIHR-RP-R3-12-027, and MRC Grant No. MR/M008894/1.

-
- [1] T. G. Walker and W. Happer, *Rev. Mod. Phys.* **69**, 629 (1997).
 [2] T. G. Vold, F. J. Raab, B. Heckel, and E. N. Fortson, *Phys. Rev. Lett.* **52**, 2229 (1984).
 [3] M. A. Rosenberry and T. E. Chupp, *Phys. Rev. Lett.* **86**, 22 (2001).
 [4] R. Jimnez-Martinez, M. Kennedy, D. J. Rosenbluh, E. A. Donley, S. Knappe, S. J. Seltzer, H. L. Ring, V. S. Bajaj, and J. Kitching, *Nat. Commun.* **5**, 3908 (2014).
 [5] L.-Q. Wang, D. Wang, J. Liu, G. J. Exarhos, S. Pawsey, and I. Moudrakovski, *J. Phys. Chem. C* **113**, 6577 (2009).
 [6] J. P. Mugler and T. A. Altes, *J. Magn. Reson. Imaging* **37**, 313 (2013).
 [7] I. C. Ruset, S. Ketel, and F. W. Hersman, *Phys. Rev. Lett.* **96**, 053002 (2006).
 [8] G. Norquay, S. R. Parnell, X. Xu, J. Parra-Robles, and J. M. Wild, *J. Appl. Phys.* **113**, 044908 (2013).
 [9] P. Nikolaou, A. M. Coffey, L. L. Walkup, B. M. Gust, N. Whiting, H. Newton, S. Barcus, I. Muradyan, M. Dabaghyan, G. D. Moroz, M. S. Rosen, S. Patz, M. J. Barlow, E. Y. Chekmenev, and B. M. Goodson, *Proc. Natl. Acad. Sci. U.S.A.* **110**, 14150 (2013).
 [10] N. D. Bhaskar, W. Happer, and T. McClelland, *Phys. Rev. Lett.* **49**, 25 (1982).
 [11] E. Babcock, I. Nelson, S. Kadlecik, B. Driehuys, L. W. Anderson, F. W. Hersman, and T. G. Walker, *Phys. Rev. Lett.* **91**, 123003 (2003).
 [12] M. S. Rosen, T. E. Chupp, K. P. Coulter, R. C. Welsh, and S. D. Swanson, *Rev. Sci. Instrum.* **70**, 1546 (1999).
 [13] G. Schrank, Z. Ma, A. Schoeck, and B. Saam, *Phys. Rev. A* **80**, 063424 (2009).
 [14] M. He, S. H. Robertson, S. S. Kaushik, M. S. Freeman, R. S. Virgincar, J. Davies, J. Stiles, W. M. Foster, H. P. McAdams, and B. Driehuys, *Magn. Reson. Imaging* **33**, 877 (2015).
 [15] S. Appelt, A. B.-A. Baranga, A. R. Young, and W. Happer, *Phys. Rev. A* **59**, 2078 (1999).
 [16] S. Appelt, T. Unlu, K. Zilles, N. J. Shah, S. Baer-Lang, and H. Halling, *Appl. Phys. Lett.* **75**, 427 (1999).
 [17] M. Abramowitz, *Handbook of Mathematical Functions, with Formulas, Graphs, and Mathematical Tables* (Dover Publications, Incorporated, New York, 1974).
 [18] T. J. Killian, *Phys. Rev.* **27**, 578 (1926).
 [19] I. A. Nelson and T. G. Walker, *Phys. Rev. A* **65**, 012712 (2001).
 [20] X. Zeng, Z. Wu, T. Call, E. Miron, D. Schreiber, and W. Happer, *Phys. Rev. A* **31**, 260 (1985).
 [21] W. Happer, E. Miron, S. Schaefer, D. Schreiber, W. A. van Wijngaarden, and X. Zeng, *Phys. Rev. A* **29**, 3092 (1984).
 [22] T. G. Walker, *Phys. Rev. A* **40**, 4959 (1989).
 [23] N. D. Bhaskar, W. Happer, M. Larsson, and X. Zeng, *Phys. Rev. Lett.* **50**, 105 (1983).
 [24] N. Ramsey, E. Miron, X. Zeng, and W. Happer, *Chem. Phys. Lett.* **102**, 340 (1983).
 [25] M. A. Bouchiat, J. Brossel, and L. C. Pottier, *J. Chem. Phys.* **56**, 3703 (1972).
 [26] G. D. Cates, R. J. Fitzgerald, A. S. Barton, P. Bogorad, M. Gatzke, N. R. Newbury, and B. Saam, *Phys. Rev. A* **45**, 4631 (1992).
 [27] See Supplemental Material at <http://link.aps.org/supplemental/10.1103/PhysRevLett.121.153201> for detailed description of polarizer apparatus.
 [28] R. Merritt, C. Purcell, and G. Stroink, *Rev. Sci. Instrum.* **54**, 879 (1983).
 [29] B. Driehuys, G. D. Cates, E. Miron, K. Sauer, D. K. Walter, and W. Happer, *Appl. Phys. Lett.* **69**, 1668 (1996).
 [30] Y.-Y. Jau, N. N. Kuzma, and W. Happer, *Phys. Rev. A* **69**, 061401 (2004).
 [31] M. S. Freeman, K. Emami, and B. Driehuys, *Phys. Rev. A* **90**, 023406 (2014).
 [32] E. Babcock, B. Chann, T. G. Walker, W. C. Chen, and T. R. Gentile, *Phys. Rev. Lett.* **96**, 083003 (2006).
 [33] M. R. Rao, N. J. Stewart, P. D. Griffiths, G. Norquay, and J. M. Wild, *Radiology* **286**, 659 (2018).
 [34] J. Chacon-Caldera, A. M. Maunder, M. Rao, G. Norquay, O. I. Rodgers, M. Clemence, C. Puddu, L. R. Schad, and J. M. Wild, Proceedings of International Society of Magnetic Resonance in Medicine, Paris, France (International Society for Magnetic Resonance in Medicine, Concord, CA, 2018), p. 4470.
 [35] P. Nikolaou, A. M. Coffey, M. J. Barlow, M. S. Rosen, B. M. Goodson, and E. Y. Chekmenev, *Anal. Chem.* **86**, 8206 (2014).
 [36] N. J. Stewart, G. Norquay, P. D. Griffiths, and J. M. Wild, *Magn. Reson. Med.* **74**, 346 (2015).

Correction: In the second sentence before Eq. (4), “Xe atom” should be “Rb atom.”

Second Correction: Minor errors in Eqs. (5)–(7) have been fixed. Coefficients given above Eq. (5) have also been corrected, along with a unit given in the caption of Fig. 2.